

On the Difficulty of Detecting Streaming Potentials Generated at Depth

PATRICK PINETTES,^{1,2,3} PASCAL BERNARD,¹ FRANÇOIS CORNET,¹
GAGUIK HOVHANNISSIAN,⁴ LAURENCE JOUNIAUX,⁵ JEAN-PIERRE
POZZI,⁵ and VÉRONIQUE BARTHÈS⁶

Abstract — In order to investigate how a streaming potential coefficient measured in the laboratory, at a typical scale of 10 cm, can be incorporated into a field model, with a typical scale of 1 to 10 km, we measured the electric field induced by water flows forced at 150 m depth through a 10 m wide granite fractured zone. The water flows were obtained by pumping cyclically 10 m of water from a borehole that cut the fractured zone at depth, and contemporaneously reinjecting it into another borehole located 50 m away. After one day, a steady-state fluid flow regime was reached, with pumping cycles lasting 45 minutes, indicating a hydraulic conductivity of 10^{-5} m s^{-1} and a specific storage coefficient of $3.25 \times 10^{-6} \text{ m}^{-1}$. The expected self-potential at the surface was an anomaly with two maxima of opposite sign and $2 \mu\text{V}$ amplitude each, both located 160 m away from the middle of the borehole heads, the signal being divided by two 500 m away from the middle of the borehole heads (in agreement with WURMSTICH and MORGAN, 1994). Instead, we observed an electrical signal of 8 mV midway between the borehole heads, and smaller than 5 mV 33 m away from the borehole heads. The discrepancy observed between the data and the model can be explained by fluid flow leakages that occurred close to the water-table head, represented about 20% of the total water flow, and activated smaller but closer electric sources. This experiment thus illustrates the practical difficulty of detecting streaming potentials generated at depth. It shows in particular that in fractured zones, and hence in the vicinity of major active fault, small water flows located far away from an energetic targeted source, but close to some of the electrodes of the network, can sometimes drastically distort the shape of the expected anomaly. Models of possible electrical earthquake precursors therefore turn out to be more speculative than expected.

Key words: Electro-kinetic phenomena, streaming potentials, self-potential, earthquake and volcanic precursors, geothermal exploration, electric methods.

1. Introduction

It has long ago been suspected that low-frequency electro-telluric and magnetic anomalies might sometimes precede tectonic events. Recently, such anomalies were observed in association with volcanic activities at La Fournaise volcano, France (ZLOTNICKI and LE MOUËL, 1990; MICHEL and ZLOTNICKI, 1998), at Mount Unzen volcano, Japan (HASHIMOTO and TANAKA, 1995), as well as in other places (see JOHNSTON, 1997 for review). Various magnetic or electric anomalies were also reported before major earthquakes (see PARK *et al.*, 1993 for review), in particular before the M_S 7.1 Loma Prieta earthquake (FRASER-SMITH *et al.*, 1990; BERNARDI *et al.*, 1991; FENOGLIO *et al.*, 1993) and, possibly, in Greece with the debated “VAN method” (LIGHTHILL, 1996).

Three questions arise from these observations: (1) Do they correspond to technical artifacts or to geophysical phenomena?; (2) If they are of geophysical origin, are they really correlated with the suspected tectonic events?; (3) If they really are associated with tectonic events, which geophysical phenomena created them?

Measurements of long term electro-telluric potentials are usually performed with so-called “non-polarizing” electrodes. A recent experiment conducted at Garchy, France, enabled a comparison of various electrode designs to be made *in situ* during one year (PERRIER *et al.*, 1997). It showed that some designs and installation methods are better than others, depending on the external conditions and the local resistivity. Furthermore, it quantified the short- (< some hours), mid- (hours to days) and long- (> days) term drifts of each design.

¹ Département de Sismologie, UMR CNRS 7580, Institut de Physique du Globe de Paris, 4 Place Jussieu, 75252 Paris cedex 05, France (e-mail: bernard@ipgp.jussieu.fr, cornet@ipgp.jussieu.fr).

² Observatoire Royal de Belgique, Avenue circulaire 3, B-1180 Bruxelles, Belgium.

³ Now at Laboratoire de Géophysique et d'Hydrodynamique en Forage, Institut des Sciences de la Terre, de l'Eau et de l'Espace de Montpellier, Université des Sciences et Techniques du Languedoc - Montpellier 2, Case courrier 56, Place Eugène Bataillon, 34095 Montpellier cedex 05, France (e-mail: pinettes.patrick@laposte.net).

⁴ Centre de Recherche en Géophysique, CNRS, 58150 Pouilly sur Loire, France.

⁵ Laboratoire de Géologie, UMR CNRS 8538, École Normale Supérieure, 24 rue Lhomond, 75 231 Paris cedex 05, France (e-mail: Laurence.Jouniaux@ens.fr, Jean-Pierre.Pozzi@ens.fr).

⁶ Laboratoire d'Électronique, de Technologies et d'Instrumentation, Division Instrumentations et Systèmes, Commissariat à l'Énergie Atomique, 17 rue des Martyrs, 38054 Grenoble cedex 9, France.

The validity of the correlations between the observations and the tectonic events can sometimes be established without any doubt, for instance, when the excitations and anomalies are repeated (see, *e.g.*, ZLOTNICKI and LE MOUËL, 1990 at La Fournaise volcano). But for scarce events like earthquakes, the correlations are generally more difficult to establish (see, *e.g.*, the purposed VAN correlations between the Greek $M > 4.5$ earthquakes and the electro-telluric observations conducted there by the VAN group, GELLER, 1996).

Many physical phenomena are known to induce electric or magnetic fields in response to tectonic stresses (see JOHNSTON, 1997 and PARK *et al.*, 1993 for review). Among them, streaming potentials (ADAMSON, 1990) appear to be the best candidate for explaining electric or magnetic anomalies induced by volcanic or earthquake activity (see ZLOTNICKI and LE MOUËL, 1990 and ADLER *et al.*, 1999 for the La Fournaise volcano; HASHIMOTO and TANAKA, 1995 for the Mount Unzen volcano; BERNARD, 1992, GRUSZOW *et al.*, 1996, PINETTES *et al.*, 1998, and PHAM *et al.*, 1998, 1999 for the VAN observations; and FENOGLIO *et al.*, 1995 for the Loma Prieta observations).

PERRIER *et al.* (1998) and TRIQUE *et al.* (1999) recently observed repeated electrical signals associated with repeated pore pressure variations induced by repeated artificial lake level variations. They showed that this observation can be explained with streaming potentials induced in a perched aquifer located below one of the electrodes. A comparison between the streaming potential coefficient required by their model and that measured in the laboratory with rock samples coming from the site confirmed the interpretation. Streaming potentials can thus generate observable potentials at the scale of hundreds of meters, with shallow sources.

The results of PERRIER *et al.* (1998) and TRIQUE *et al.* (1999) do not teach us anything regarding the possible ability of streaming potentials to generate observable anomalies with deep buried sources (> 100 m). The physical conditions at depth are generally far different from that in the laboratory (different pH , temperature, pressure and characteristic lengths, etc.). So the only way to model data coming from such situations consists in extrapolating results from standard laboratory experiments (*e.g.*, ISHIDO and MIZUTANI, 1981; MORGAN *et al.*, 1989; JOUNIAUX and POZZI, 1995, 1997; LORNE *et al.*, 1999a, b).

REVIL *et al.* (1999a, b) recently derived a general formal theory of streaming potentials in porous media. Their model depends on many assumptions. It is in particular restricted to temperatures lower than about 100°C . BERNABÉ (1992) made theoretical experiments to test the upscaling of electro-kinetic phenomena for heterogeneous media. He showed that several discrepancies are expected between the micro- and macroscopic equations. Moreover, he found that the electrical current and potential gradients should be much more localized in highly heterogeneous networks than in homogeneous ones. He did not investigate the effects of temperature and pressure. Using a finite-difference approach for modeling steady-state streaming potentials generated by standard oil well pumping in typical North American reservoirs ($500\text{ m}^3\text{ day}^{-1}$ pumpings of 100 m wide reservoirs buried at 500 m depth with a streaming potential coefficient of 100 mV MPa^{-1} , a permeability of 150 mD and a resistivity of $50\ \Omega\text{ m}$), WURMSTICH and MORGAN (1994) showed that bell-shape potential anomalies are expected at the surface, with a maximum of the order of $500\ \mu\text{V}$ close to the production well, and a rapid decay of the signal away from the well (amplitude divided by 5 about 3 km away from the well). ISHIDO and PRITCHETT (1999) recently tested the effect of a dilatant strain inducing 20 MPa of depression 6 km around a vertical fault zone of 5 km width, 4 km height, 10 m thickness and 7 km depth. They showed that signals up to 60 mV km^{-1} are expected at the surface, provided that a 0.1 S m^{-1} conductive channel of 1 km width and 100 m thickness is present from 100 m below the surface down to the fault zone depth.

None of these upscalings are presently controlled by direct *in situ* measurements. In fact, the available data are restricted to poorly constrained experiments, like that of ISHIDO *et al.* (1983), who measured the self-potential generated at the surface of hot water eruptions induced by sudden openings of head valves of 700 m deep cased wells in the Takinoue geothermal area, Japan. They observed signals of the order of 5 mV with electric lines located 20 and 150 m away from the production wells. This observed value is bigger than the calculations of WURMSTICH and MORGAN (1994), but the reservoir was deeper and thicker than that tested by WURMSTICH and MORGAN (1994) (600 and 200 m respectively). The permeability and resistivity were furthermore ten times smaller than that tested by WURMSTICH and MORGAN (1994). ISHIDO *et al.* (1983) explain their result with crude assumptions, for example that the electrical currents are supposed purely horizontal and radial. They conclude that the streaming potential coefficient at the source is 5 times smaller than that tested by WURMSTICH and MORGAN (1994), but they do not confirm it with direct measurement, and they do not investigate the effect of diphasic flows, that are likely to occur at depth and that are known to enhance the streaming potentials (*e.g.* MORGAN *et al.*, 1989).

While theories extrapolated from laboratory experiments are in agreement with field experiments when the sources are superficial, discrepancies thus still exist in the case of buried electric sources, in particular when the media are heterogeneous or fractured. Experimental studies enabling the signal generated at the surface by streaming potentials induced at depth through fractured media to be constrained are therefore required.

The aim of the present study is to investigate this very last point, by presenting the results of an experiment conducted in 1996, in a granite area, and consisting of the measurement of the electric potential generated at the surface and at depth by forced water flows induced at 150 m depth, through a 10 m wide sub-horizontal fractured zone. After a brief description of the experiment, we show that streaming potentials were observed in association with the hydraulic excitations. A detailed quantification of the model generally proposed for explaining them shows that the surface measurements cannot be explained by the targeted deep electric source. They were rather due to smaller but shallower streaming potential sources, incidentally activated and whose effects dominated at the surface. These results have fundamental implications in earthquake precursors research.

1. The Mayet de Montagne experiment of September 1996

The test site at the Mayet de Montagne is located in central France, 25 km to the south-east of Vichy. It was originally chosen in 1984 for conducting large-scale *in situ* experiments on forced water circulations in a granite area (CORNET, 1988). Eight 200 m or more deep boreholes were drilled in granite and cut a major sub-horizontal altered zone located at about 150 m depth (Fig. 1a). The average thickness of this zone is 8 m, as attested by its thermal signature (Fig. 1b). At the surface, the distance between the boreholes is of the order of 50 m (Fig. 2).

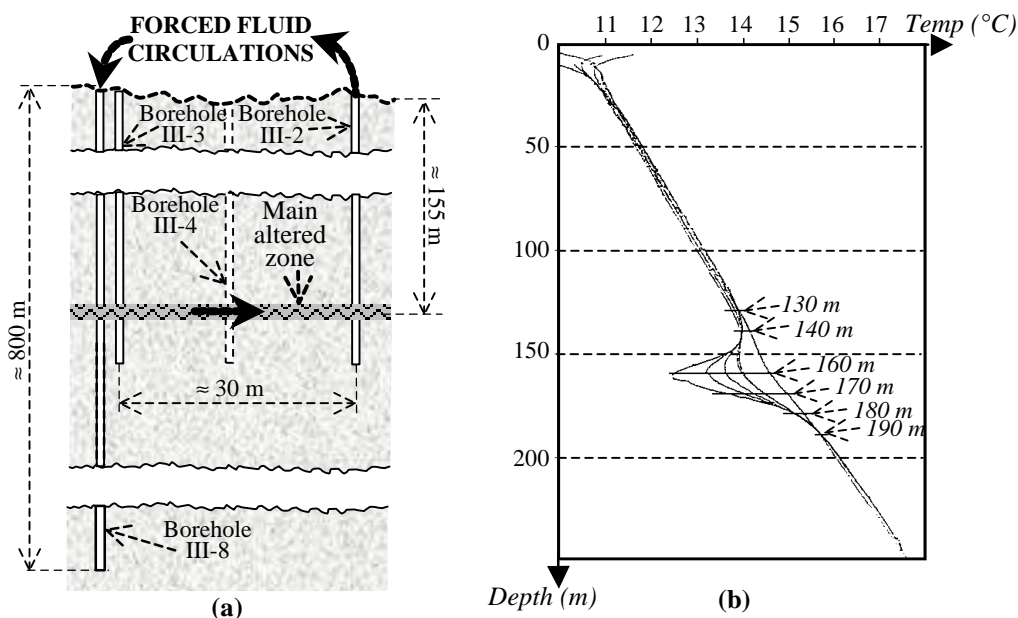


Figure 1
(a) Schematic cross section of the aquifer and the instrumented boreholes. Less active sub-horizontal aquifers are present, though not represented. (b) Available thermal soundings at borehole III-4 (1982/06/03, 1982/09/14, 1983/04/27 and 1983/05/18). From CORNET (1984, Fig. 21).

At the beginning of the experiment, the sub-surface water level was -8.4 m in borehole III-2 and -13.7 m in boreholes III-3 and III-8. The fluid circulation through the altered zone was forced by pumping water regularly from borehole III-2 and reinjecting it immediately in borehole III-8 via a standard plastic pipe installed between the borehole heads. The flow was driven by a down-hole electric pump placed 29.9 m down borehole III-2. The pump was programmed to start pumping automatically when the water level in this well reached -18.2 m, and to stop when the water level fell to -28.2 m. The pump rate during the pumping periods was constant and equal to about 2.15 l s^{-1} . One day and a half after the beginning of the experiment, a steady-state fluid flow regime was reached, with pumping periods lasting $101 \text{ s} \pm 1 \text{ s}$, and pumping cycles lasting $45' 5'' \pm 30 \text{ s}$.

In order not to induce too much electric noise close to borehole III-2, the pump was automatically isolated from the local 220 V power supply network whenever it was off (*i.e.*, $43' 24''$ during each $45' 5''$ pumping cycle, *i.e.*, 96.3% of the time). The pipe between boreholes III-2 and III-8 was electrically insulated, and no permanent water was present at the surface (either anthropogenic or as rainfall). Thus, there was no electrical connection at the surface between boreholes III-2 and III-8, except possibly during some seconds when the pump was active and when water was forced to fall from borehole III-8 head into the water table head there. Boreholes III-2, III-3, III-4 and III-6 were not cased, and borehole III-8 was cased only from 165 m on (hence, deeper than the altered zone).

The surface electrode network was sized according to the *a priori* characteristic length of the experiment, that is the aquifer depth, 150 m (Fig. 2). In addition, two electrodes were installed in borehole III-3, at 137 m and 152 m depths, in order to sample the vertical electric field. An active resistive barometer was installed 30 m down in borehole III-3, in order to measure the water level 8 m to the south-east of borehole III-8 (see Fig. 2). The activity of the pump was also recorded.

The electrodes were made of Pb/PbCl₂ with a kaolinite absorber (CLF-Na design of PERRIER *et al.*, 1997, Table 1). They were installed in opened plastic buckets filled with local soil with NaCl in excess saturation, and buried at an average depth of 50 cm (PERRIER *et al.*, 1997, Fig. 1b). The maximum possible drift is expected to be of the order $5 \mu\text{V/day}$ (PERRIER *et al.*, 1997, Fig. 4).

The voltage differences between each electrode and the reference electrode ERR0 were measured by an IOtech DaqBook 216. Fourteen of its single-ended inputs were connected to its internal 16 bits over $\pm 5 \text{ V}$ Analog-to-Digital Converter. The instrument was programmed to work at 10 Hz, without anti-aliasing analog filters between the electrodes and the analog input. The connection between the electrodes and the acquisition

system was ensured *via* wires soldered to the electrode wires and protected by self-amalgamating strips. The input impedance presented to the electrodes was that of the logger, *i.e.*, $100\text{ M}\Omega$ in parallel with 100 pF (see full specifications of the DaqBook 216 at IOTech web site: <http://www.iotech.com/catalog/daq/daqbook.pdf>).

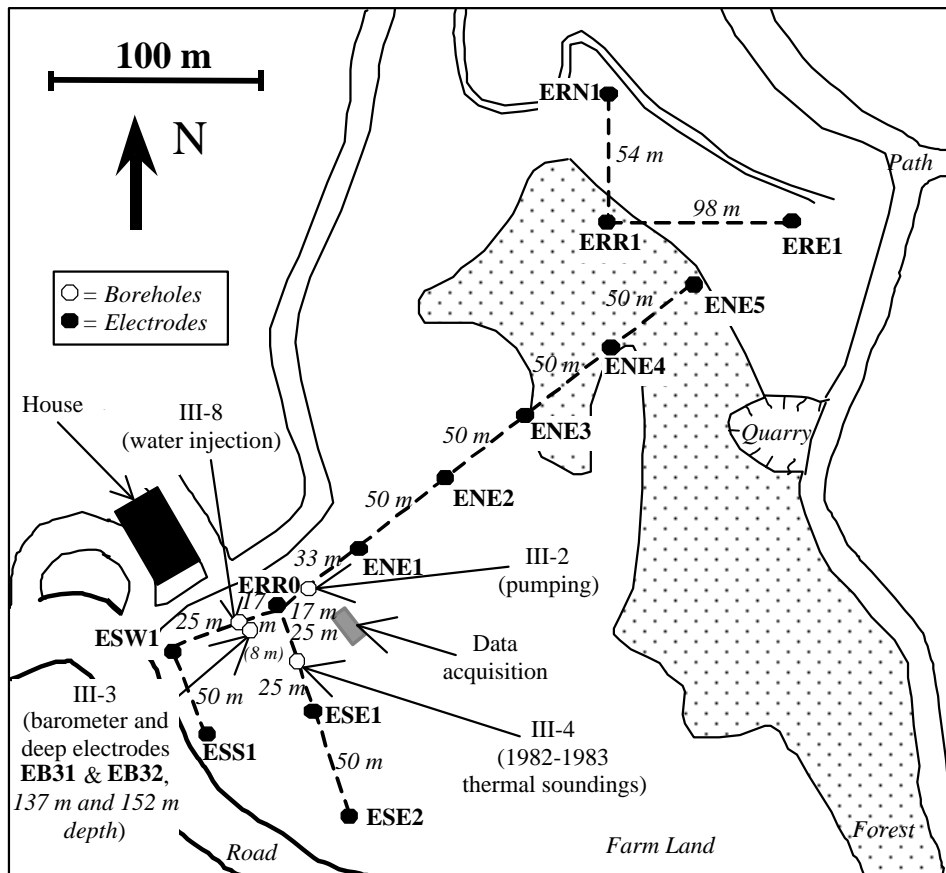


Figure 2

Schematic view of the experiment. The electrodes are located in 5 m radius circles centered on the points. The site was originally chosen for conducting large scale *in situ* experiments on forced water circulations in a granite area (CORNET, 1988)

The signals coming from the barometer and the pump were digitized by another data logger, a Data Electronics Datataker DT500. This logger had two differential analog inputs connected to its internal 16 bits over $\pm 2.5\text{ V}$ Analog-to-Digital Converter, and was programmed to work at 1 Hz (see full specifications of the DT500 at the Data Electronics web site: <http://www.datataker.com/downloads/products/DT500600new.pdf>).

The data were saved in two passes: (i) at first, in real time, in the internal buffer memory of the loggers; (ii) then with a delay of some seconds for the DaqBook and of some hours for the Datataker, in the hard disk of portable PCs that were connected to the loggers *via* parallel ports. All the loggers and the PCs, as well as the barometer, were powered by three 12 V 38 Ah batteries, where those of the PCs were permanently on charge *via* standard 12 V car battery chargers connected to the local 220 V power supply network.

2. Observations

The Mayet de Montagne site is located on farm land, with many electrical fences in activity in the vicinity. In order to test the possible effect of these electrical fences on the local electric noise, we stopped the closest one (located about 50 m to the south-east of our experiment) for half an hour, and compared the signals measured before and during the test. The corresponding data are presented Fig. 3 in terms of power spectra. It can be seen that quite significant noise is present between 2 and 15 s, which is partially contributed by the electrical fences. This noise is however not expected to produce aliasing of the data provided that the sampling frequency is greater than 1 Hz, which is the case in all the data presented in this paper.

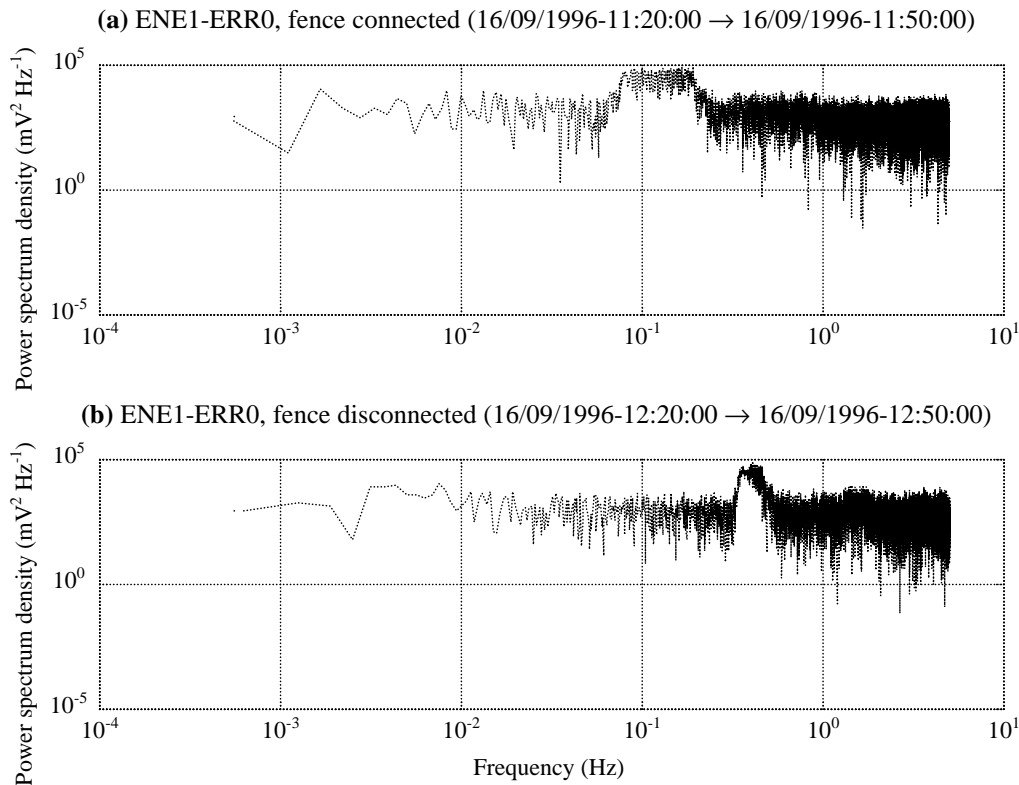


Figure 3

Power spectrum of the voltage differences between electrodes ENE1 and ERR0 during 20 minute periods. (a) Period during which the closest electrical fence was connected. (b) Period during which it was not connected.

The power spectra from measurements between the electrodes in borehole III-3 (EB31 and EB32) were also measured when the closest electric fence was connected, and then disconnected. The results are similar to that of Fig. 3. The noise observed at the surface was therefore not significantly attenuated with depth, down to 150 m. This indicates either that an important part of the noise is generated close to the aquifer (for instance close to a borehole filled with water up to the surface and well connected with the aquifer at 150 m depth), or that it is induced in the logging wires close to the surface.

The electric potential of all the electrodes referenced to electrode ENE5 are presented in Fig. 4 for the total duration of the experiment. Similar curves are obtained when the reference is changed to any electrode, except ERE1 or ESS1. It turns out that all the electrodes but ERE1 and ESS1 are stable and have a behavior compatible with the observations of PERRIER *et al.* (1997). The visible drift on electrode ESS1 during the first three hours probably corresponds to a stabilization problem. It is not important since it has a total amplitude of about 25 mV and eventually vanishes. The long term drift visible on electrode ERE1 is, on the contrary, serious, since it has a total amplitude of about 200 mV and never vanishes. The data coming from that electrode are thus excluded.

The electric potentials expected at the surface in response to our excitations are of the order of fractions of μV , as detailed later. Such signals clearly cannot be detected directly in the raw data, where the noise level is thousands of times bigger in amplitude (Fig. 4). Indeed, an eye comparison in the time domain between the pressure and electrical signals does not reveal any visible correlation between any electrical signal and the pressure or pump signals. Yet, as our excitation is characterized in the frequency domain by a single peak at 45 minutes plus its harmonics, a better signal-to-noise ratio is expected in the spectral domain. We thus compared the power spectrum of the pressure with the power spectra of some of the voltage differences, and it revealed common peaks at 45 minutes for the pressure and all the voltage differences that include electrode ERR0 (Fig. 5). A less defined peak could also be seen on ESW1-EB32 and ESW1-EB31 data, once again at 45 minutes.

The signals detected at 45 minutes can be due either to streaming potentials induced by the forced fluid circulations, or to artificial noises induced by possible electrical leakage of the electric pump. In both cases, the periodicity of the expected noise is of the order of 45 minutes, but while in the former case its duration should be governed by the duration of the fluid flows (*i.e.*, 45 minutes), in the latter case it should be governed by the duration of the possible electrical leakage (at most 100 s, see Section 1). We looked at the data in the time domain, after having stacked them on each pumping cycle except the perturbed ones (cycles 2 3 8 9 10 15 of Fig. 4). The corresponding results are presented Fig. 6. The signal that generates the peak visible at 45 minutes in the spectra is clearly visible on ERR0-ENE1 and ERR0-ESW1 (Fig. 6a, b). It lasts about 45 minutes, so it cannot be due to the pump. It moreover cannot be due to a filter effect, as the data were filtered at 250 s before the stack,

i.e., at a period which is negligible compared to the duration of the excitation (45 minutes). Consequently, it is very likely that this signal corresponds to streaming potentials induced by the forced fluid circulations.

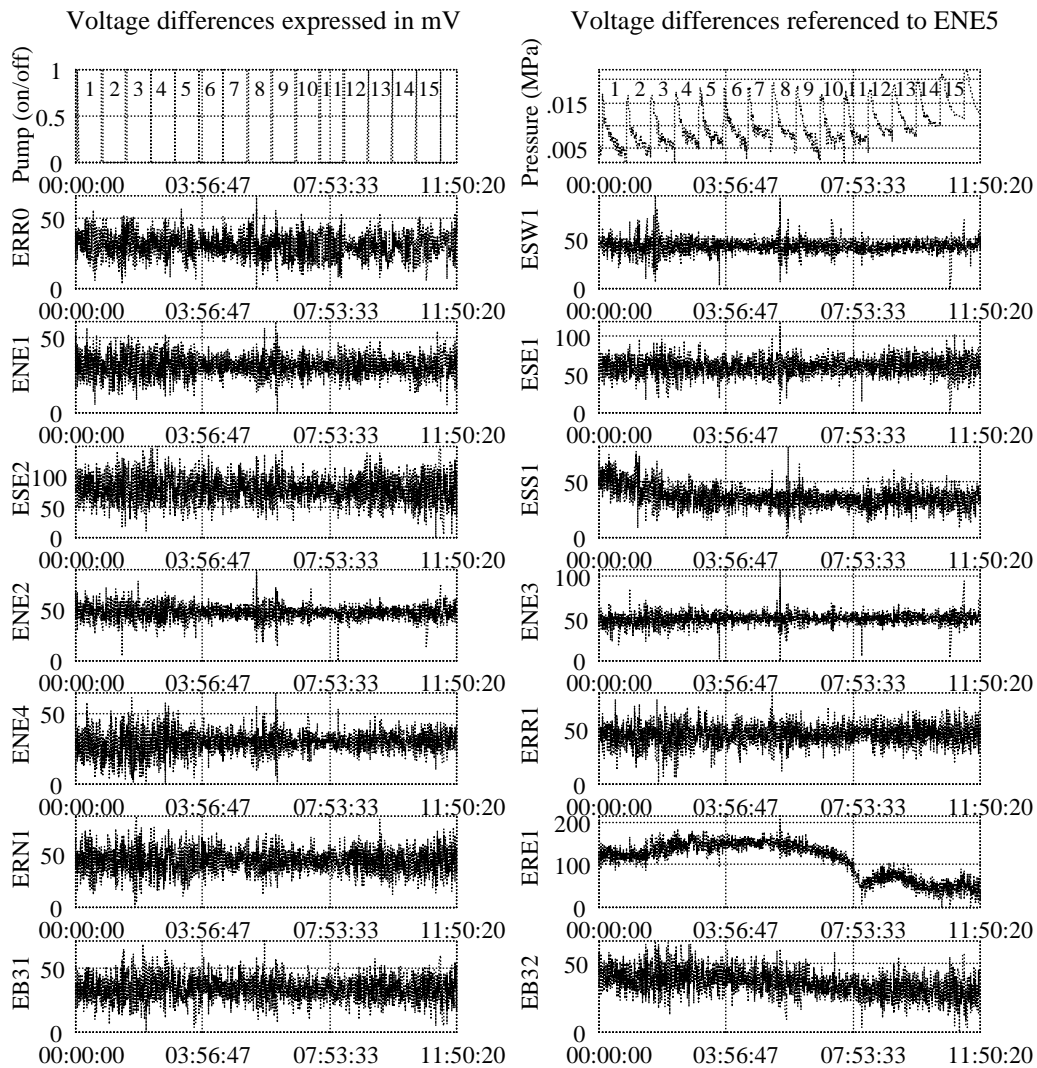


Figure 4

Electric potential of all the electrodes referenced to electrode ENE5. The monitorings began on 1996/09/25-18:45:50, after the steady-state fluid flow regime was reached. The data, originally sampled at 10 points per second for the electric potentials and at 1 point per second for the pump and pressure signals, were filtered at 50 s with a sixth-order non-dephasing low-pass Butterworth filter and roughly desampled to 1 point every 10 seconds. The long term drift visible on the pressure signal is not significant, since it is due to the slow discharge of the standard 12 V battery that was powering the instrument during the experiment. The long term drift visible on electrode ERR1 on contrary reveals a severe problem, which lead us to reject the data. The slow stabilization visible on electrode ESS1 during the first three hours of measurements, as well as the high frequency noises visible during cycles number 2, 3, 8, 9, 10 and 15, are not important, and do not imply rejection of the data.

No signal corresponding to the peak visible at 45 minutes in the spectra of ERR0-ESE1 can be seen on ERR0-ESE1 (Fig. 6c). We therefore cannot conclude whether this peak is due to streaming potentials induced by the forced fluid circulations, or to any other electric source.

The time signals corresponding to the 45 minute peaks appearing in the power spectra of ESW1-EB32 and ESW1-EB31 are hardly detectable in Fig. 6f and g. Yet, a close look at the data reveals a small signal that emerges slightly from the noise during the first 7 minutes of the monitoring (Fig. 6f and g). As it lasts longer than 250 s, it very likely corresponds to streaming potentials induced by the forced fluid circulations.

The reason why the EB31-EB32 combination does not monitor any signal is due to the fact that EB31 and EB32 are installed in the same borehole, close to each other (15 m), so that they are permanently short circuited. On contrary, ESW1 and EB32 and EB31 are separated by the granite bedrock, which is resistive enough so as not to cancel the electric potential present between the electrodes.

The amplitudes of the signals detected in association with the forced fluid circulations were of the order of 5 mV for ERR0-ENE1, 8 mV for ERR0-ESW1 and 2.5 mV for ESW1-EB32 and ESW1-EB31 (Fig. 6a, b, f and g).

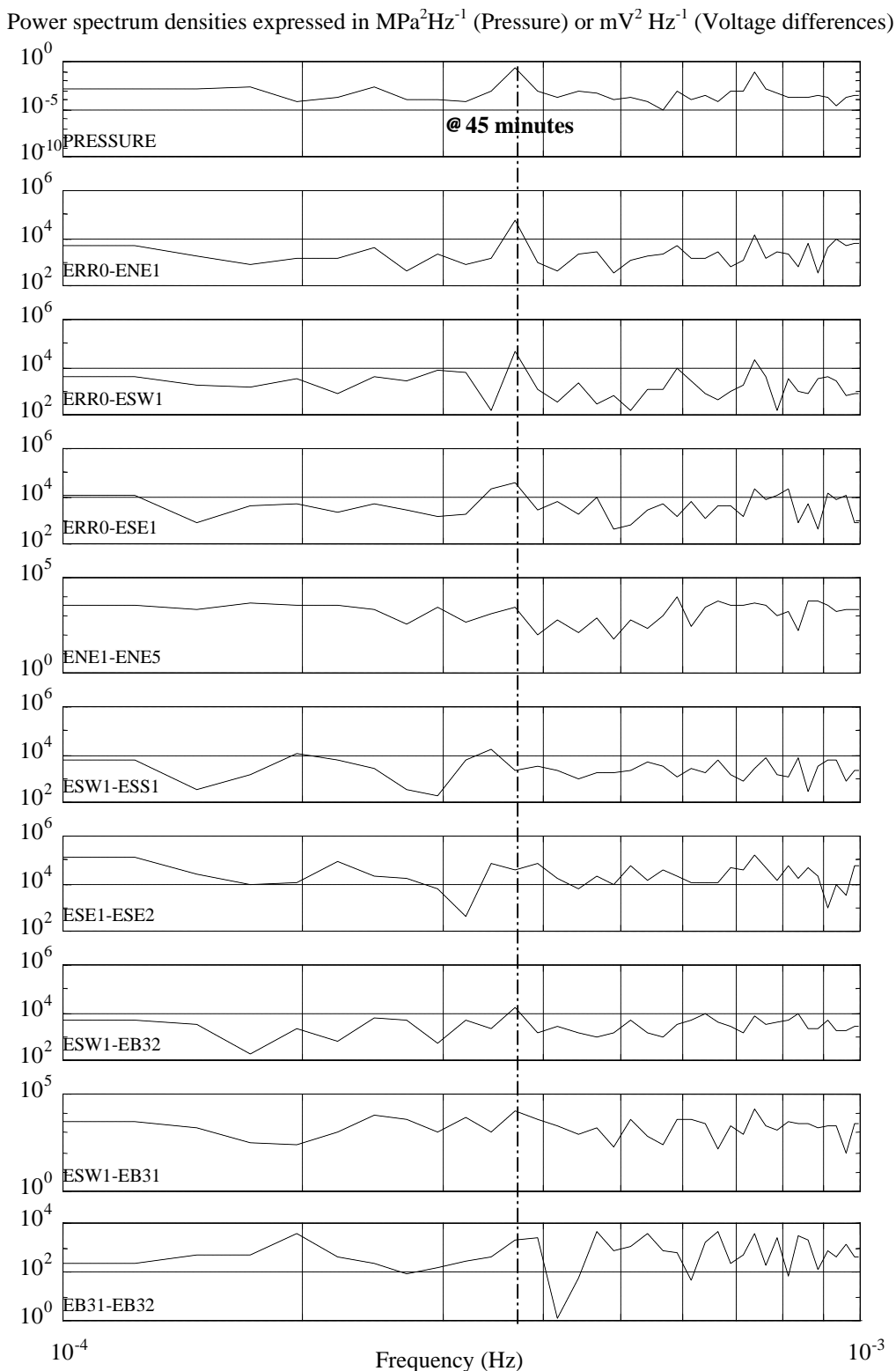


Figure 5

Power spectra of the pressure and some of the measured voltage differences between 1996/09/25-18:48:13 and 1996/09/26-06:05:09 (hence during the total duration of the experiment). The data, originally sampled at 10 points per second for the electric fields and at 1 point per second for the pressure, were filtered at 50 s with a sixth-order non-dephasing low-pass Butterworth filter and roughly desampled to 1 point every 10 seconds, before the estimation of the spectra. Frequency picks at 45 minutes are clearly visible in the pressure, ERR0-ENE1, ERR0-ESW1 and ERR0-ESE1 signals. Smaller picks appear at the same frequency for ESW1-EB32 and ESW1-EB31.

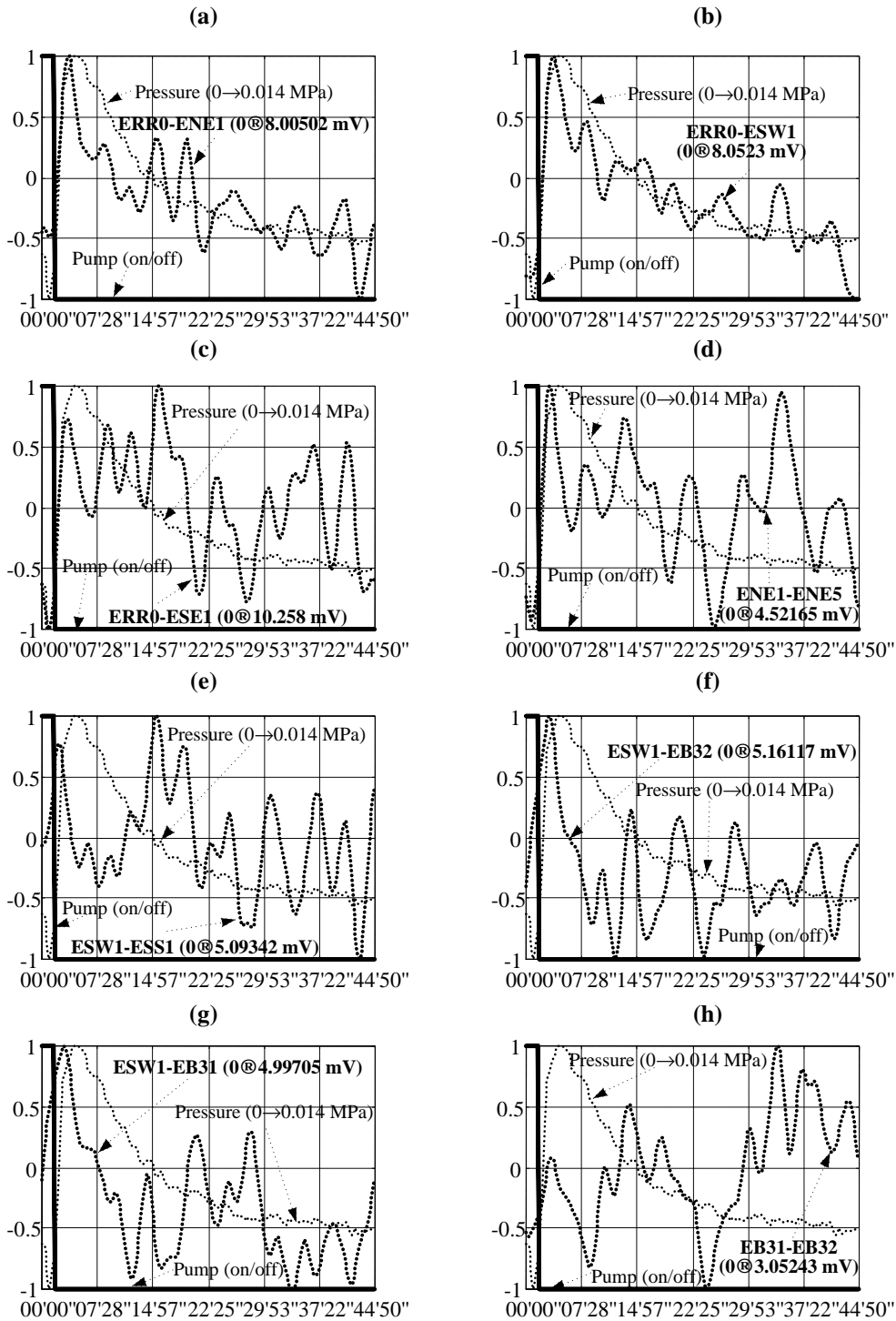


Figure 6

Pressure and voltage differences stacked on each pumping cycle but the perturbed ones (cycles 1 2 3 8 9 10 15 removed). The data, originally sampled at 1 point per second for the pressure and the pump (respectively 10 points per second for the voltage differences), were filtered at 50 s (respectively 250 s) with a sixth-order (respectively fourth-order) non-dephasing low-pass Butterworth filter, and roughly desampled to 1 point every 10 seconds. A signal lasting about 45 minutes is clearly visible on ERR0-ENE1 and ERR0-ESW1, and another one lasting about 7 minutes slightly emerges from the noise on ESW1-EB32 and ESW1-EB31.

3. Modeling

When a fluid is forced to percolate through a permeable rock, an electrical current appears. It is called the *convection current*. It is proportional to the pressure gradient

$$\overrightarrow{j}_{conv} = \frac{\mathbf{e} \times \mathbf{V}}{\mathbf{h}} \times \overrightarrow{\nabla}(P) = C \times \mathbf{s} \times \overrightarrow{\nabla}(P), \quad (1)$$

where \mathbf{e} is the dielectric constant of the fluid, \mathbf{z} is the zeta potential of the fluid/rock interface, \mathbf{h} is the dynamic viscosity of the fluid and P is the pressure (C being the streaming potential coefficient and \mathbf{s} the electrical conductivity of the fluid). Such an electrical current creates an electric potential V , which in turn creates a second electrical current, the *conduction* current, that is proportional to the potential gradient

$$\overrightarrow{j}_{cond} = -\mathbf{s} \times \overrightarrow{\nabla}(V) \quad (2)$$

and that tends to cancel the convection current. The total electric charge is conservative, so when the permanent electric regime is reached, and in absence of any other electrical current source, the divergence of the total electrical current is equal to zero

$$\overrightarrow{\nabla}[\mathbf{s} \times \overrightarrow{\nabla}(V)] = \overrightarrow{\nabla}[C \times \mathbf{s} \times \overrightarrow{\nabla}(P)]. \quad (3)$$

Though the altered zone is intrinsically fractured, it can be approximated with an equivalent continuous porous medium (DE MARSILY, 1986, pp. 65-72). The volume fluid flow thus contains two terms. One is proportional to the gradient pressure

$$\overrightarrow{J}_{Darcy} = -\frac{\mathbf{k}}{\mathbf{h}} \times \overrightarrow{\nabla}(P), \quad (4)$$

where \mathbf{k} is the rock permeability. The other one is proportional to the second force of the system, the potential gradient

$$\overrightarrow{J}_{osmo-electric} \propto \overrightarrow{\nabla}(V). \quad (5)$$

According to the Onsager reciprocal relations, the coefficients in Eqs. (1) and (5) must be the same (DE GROOT and MAZUR, 1962), so

$$\overrightarrow{J}_{osmo-electric} = C \times \mathbf{s} \times \overrightarrow{\nabla}(V). \quad (6)$$

In the altered zone of the Mayet de Montagne, \mathbf{k} can be estimated to be of the order of 10^{-12} m^2 (Fig. 7), \mathbf{h} about 10^{-3} Pa s (the water was approximately at 20°C), $\mathbf{s} = 3.2 \times 10^{-2} \text{ S m}^{-1}$ (measured directly in the field), C about 100 mV MPa^{-1} (ISHIDO and MIZUTANI, 1981; MORGAN *et al.*, 1989; JOUNIAUX and POZZI, 1995, 1997; LORNE *et al.*, 1999a, b), $\|\overrightarrow{\nabla}(P)\|$ between $10^{-2} \text{ MPa m}^{-1}$ and 10 Pa m^{-1} (Fig. 8b and Eq. (1)), and $\|\overrightarrow{\nabla}(V)\|$ at most 0.6 mV km^{-1} (Fig. 12 at 137 m depth). $\|\overrightarrow{J}_{Darcy}\|$ is thus expected to be between $10 \text{ } \mu\text{m s}^{-1}$ and 10 nm s^{-1} , while $\|\overrightarrow{J}_{osmo-electric}\|$ is expected to be at most of the order of $1.8 \times 10^{-15} \text{ m s}^{-1}$, *i.e.*, always negligible with respect to $\|\overrightarrow{J}_{Darcy}\|$. Hence, the hydraulic and electric problems can be solved independently.

The altered zone behaves like a confined aquifer. With the hydraulic head h defined as $h = \frac{P}{\mathbf{r} \times \mathbf{g}} + z$, where P is the pressure, \mathbf{r} the mass of water per unit volume, \mathbf{g} the acceleration due to gravity, and z the elevation measured positively upwards, it therefore follows (DE MARSILY, 1986, Chapter 5.3) that

$$\overrightarrow{\nabla}^2(h) = \frac{S}{T} \times \frac{\partial h}{\partial t} + \frac{Q_s}{T}, \quad (7)$$

where Q_s is the water flow rate per unit surface area withdrawn from the aquifer and $S = S_s \times e = \mathbf{r} \times \mathbf{g} \times \mathbf{f} \times \left(\mathbf{b}_f - \mathbf{b}_s + \frac{\mathbf{a}}{\mathbf{f}} \right) \times e$, the storage coefficient of the aquifer. Here S_s is the specific storage coefficient, \mathbf{f} is the porosity, \mathbf{b}_f , \mathbf{b}_s and \mathbf{a} are the fluid, mineral and soil compressibility coefficients, and e is the aquifer thickness. The parameter $T = K \times e = \frac{\mathbf{k} \times \mathbf{r} \times \mathbf{g}}{\mathbf{h}} \times e$ is the aquifer transmissivity, where K is the hydraulic conductivity.

No analytical solution of Eq. (7) is known for the present geometry, with two boreholes. But as noted by DE MARSILY (1986, pp. 190-191), CARLSAW and JAEGER (1986, pp. 341-344) derived a particular solution for the analog heat conduction problem with one borehole only. PAPAPOULOS and COOPER (1967) adapted this solution to hydrogeology for $r = a$, when a constant fluid flow rate Q is withdrawn from a confined aquifer of thickness e , storage coefficient S and transmissivity T , through a borehole of radius a . The hydraulic head then follows $h(r,t)$

$$\frac{2}{p^2} \times \frac{S \times Q}{T} \times \int_0^\infty du \times \left[1 - \exp\left(-\frac{T}{S} \times \frac{t}{a^2} \times u^2\right) \right] \times \frac{J_0\left(\frac{r}{a} \times u\right) \times \left[u \times Y_0(u) - 2 \times S \times Y_1(u) \right] - Y_0\left(\frac{r}{a} \times u\right) \times \left[u \times J_0(u) - 2 \times S \times J_1(u) \right]}{u^2 \times \left\{ \left[u \times J_0(u) - 2 \times S \times J_1(u) \right]^2 + \left[u \times Y_0(u) - 2 \times S \times Y_1(u) \right]^2 \right\}} \quad (8)$$

where J_n and Y_n are the Bessel functions of the first and second kinds, of the order n . This solution is adapted to our problem, since we want to estimate the first order of the hydraulic head, and the induced hydraulic head step is equal to 10 m, while the distance between the boreholes is equal to more than three times 10 m, *i.e.*, it is always large compared to the influence distance between one borehole and the other.

In the Mayet de Montagne, $a = 8.25$ cm, $Q = 2.15$ l s⁻¹, and $e = 8$ m. The only unknowns of the hydrogeological problem were thus the equivalent specific storage coefficient S_{seq} and the equivalent hydraulic conductivity K_{eq} of the altered zone. We determined them by comparing the pressure measured in borehole III-3 with the results of numerical estimates of Eq. (8) with S_{seq} varying from 10⁻⁷ to 10⁻² m⁻¹, and K_{eq} varying from 10⁻⁹ to 10⁻² m s⁻¹. The best fit was found for $S_{seq} = 3.25 \times 10^{-6}$ m⁻¹ and $K_{eq} = 10^{-5}$ m s⁻¹ (Fig. 7). Taking $h = 1.002 \times 10^{-3}$ Pa s, $g = 9.81$ m s⁻², $r = 10^3$ kg m⁻³, $b_f = 5 \times 10^{-10}$, $b_s = 2 \times 10^{-11}$ Pa⁻¹ (DE MARSILY, 1986, p. 108), these values correspond to an equivalent soil compressibility $a_{eq} = 3.3 \times 10^{-10}$ Pa⁻¹ and an equivalent permeability $k_{eq} = 1$ D (so that $f_{eq} \times b_f \ll a_{eq}$ whatever the equivalent porosity f_{eq}). This value of S_{seq} implies that it is dominated by the soil compressibility, so the ability of the Mayet de Montagne aquifer to store water is controlled by the rock matrix compressibility and not by the fluid or mineral compressibility. Such values of S_{seq} and K_{eq} are realistic for a granite fractured zone (DE MARSILY, 1986, Chapter 5).

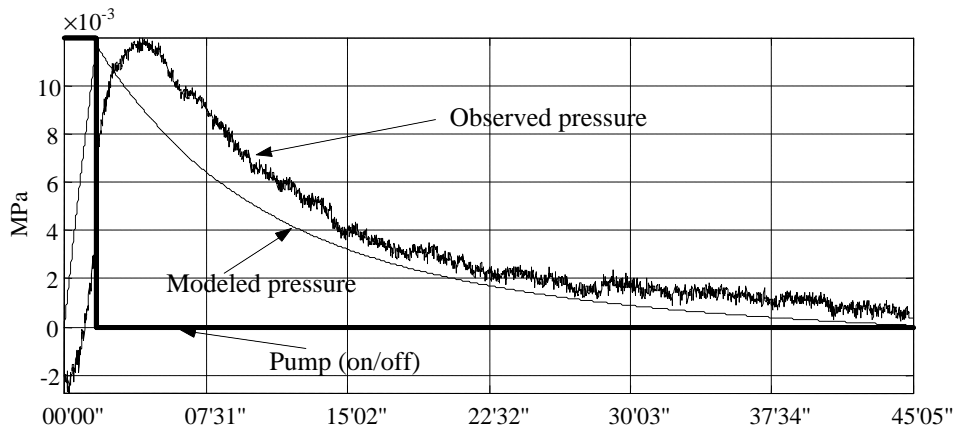


Figure 7

Modeled pressure after 14 fluid injections and for $S_{seq} = 3.25 \times 10^{-6}$ m⁻¹ and $K_{eq} = 10^{-5}$ m s⁻¹ (that is for $a_{eq} \approx 3.3 \times 10^{-10}$ Pa⁻¹ — so that $f_{eq} \times b_f \ll a_{eq}$ whatever f_{eq} — and $k_{eq} \approx 1$ D) and observed pressure after stacking on 15 pumping cycles in borehole III-3. The data are sampled at 1 point per second.

Two important points should be emphasized at this step of the modeling. It can be seen Fig. 7 that the pressure measured into borehole III-3 does not immediately grow after water is injected in borehole III-8. It first drops, by about 0.0025 MPa in about 15 s, before it finally grows, with a delay of about 1 minute with respect to the modeled pressure. At the end of the pumping cycle, the pressure in borehole III-3 is equal to its level immediately before water was injected into borehole III-8. It is possible that the first minute drop may be due to fractures located in the vicinity of borehole III-3 put in tension when water is injected into borehole III-8 and

sucking water from borehole III-3 when the drained regime between boreholes III-8 and III-3 is not yet established (Fig. 9).

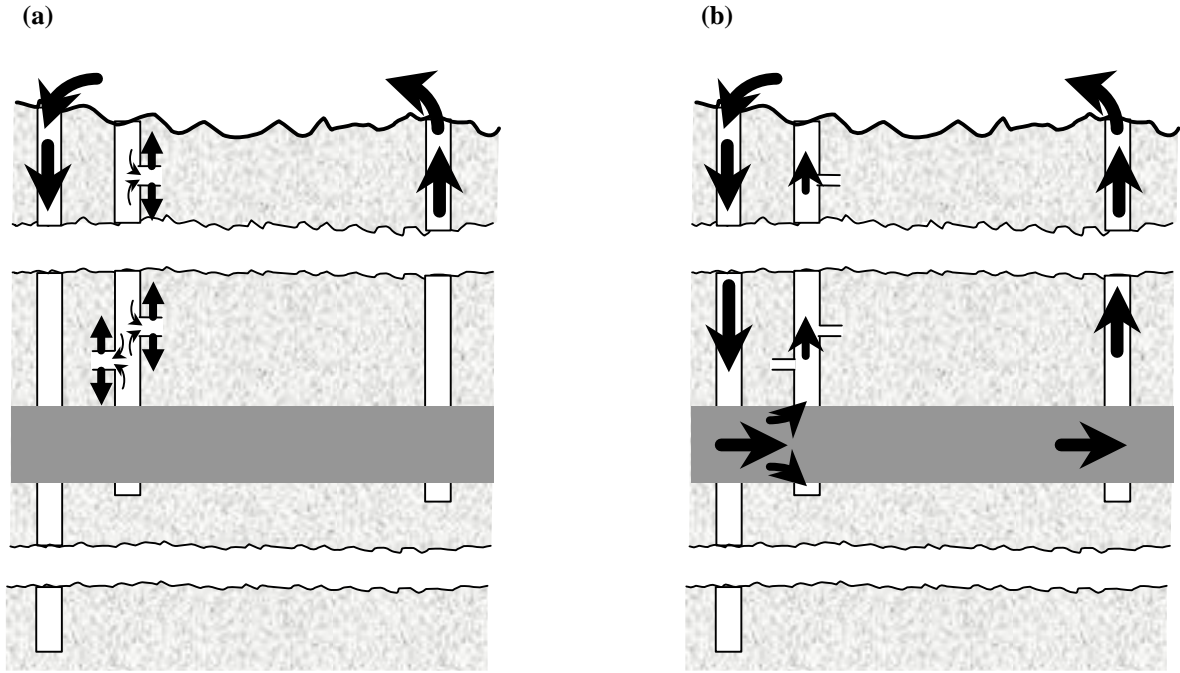


Figure 9

(a) At first, during the first minute of the water injection in borehole III-8, the drained regime in the aquifer is not established yet, and the fractures that are located in the vicinity of borehole III-3 are put in tension and suck water from borehole III-3. The pressure in borehole III-3 drops down. (b) One minute after the water injection in borehole III-8, the drained regime in the aquifer (or in fractures interconnecting boreholes III-8 and III-3) is established, so that water is drained from borehole III-8 to borehole III-3, and makes the pressure in borehole III-3 increase.

The second point that should be emphasized is the fact that the maximum pressure measured in borehole III-3 is equal to 0.016 MPa, while we expected *a priori* a greater signal, of the order of less than 0.1 MPa, that is the height of water injected in borehole III-8. The maximum pressure at $r = a$ deduced from the numerical simulations of Eq. 8 (0.02 MPa) confirms this impression, as it is much smaller than the maximum pressure *a priori* induced in borehole III-8 (about 0.1 MPa). It shows that borehole III-8 obviously does not behave like borehole III-2, probably because, unlike borehole III-2, it is drilled down to 780 m, so that it is connected to deeper aquifers, which clearly absorb a significant part of the water withdrawn from borehole III-2. The induced fluid flow is therefore less symmetric than expected.

In the altered zone, C and \mathbf{S} can be assumed constant. Eq. (3) thus becomes

$$\vec{\nabla}^2(V) - C \times \vec{\nabla}^2(P) = 0. \quad (9)$$

By analogy with the standard Poisson equation (which is valid here because the electric conductivity is of the order of 10^{-2} S m^{-1} and the characteristic times are greater than 1 min, so that $\frac{\mathbf{S}}{\mathbf{w} \times \mathbf{e}} \gg 1$, where \mathbf{w} is the pulsation), an equivalent volumetric electric charge $\mathbf{r}_{e(r,t)}$ thus develops where the pressure Laplacian is not negligible

$$\mathbf{r}_{e(r,t)} = -\mathbf{e} \times C \times \vec{\nabla}^2(P), \quad (10)$$

that is, according to Eq. (7) and to the definition of the hydraulic head

$$\mathbf{r}_{e(r>a,t)} = -\mathbf{r} \times g \times \mathbf{e} \times C \times \frac{S}{T} \times \frac{\partial h}{\partial t}. \quad (11)$$

In the case where there is one borehole only, $\mathbf{r}_{e(r,t)}$ can be derived from $h_{(r,t)}$ curves calculated with Eq. (8) and $S_{seq} = 3.25 \times 10^{-6} \text{ m}^{-1}$ and $K_{eq} = 10^{-5} \text{ m s}^{-1}$. With C negative, $\mathbf{r}_{e(r,t)}$ is positive close to borehole III-8

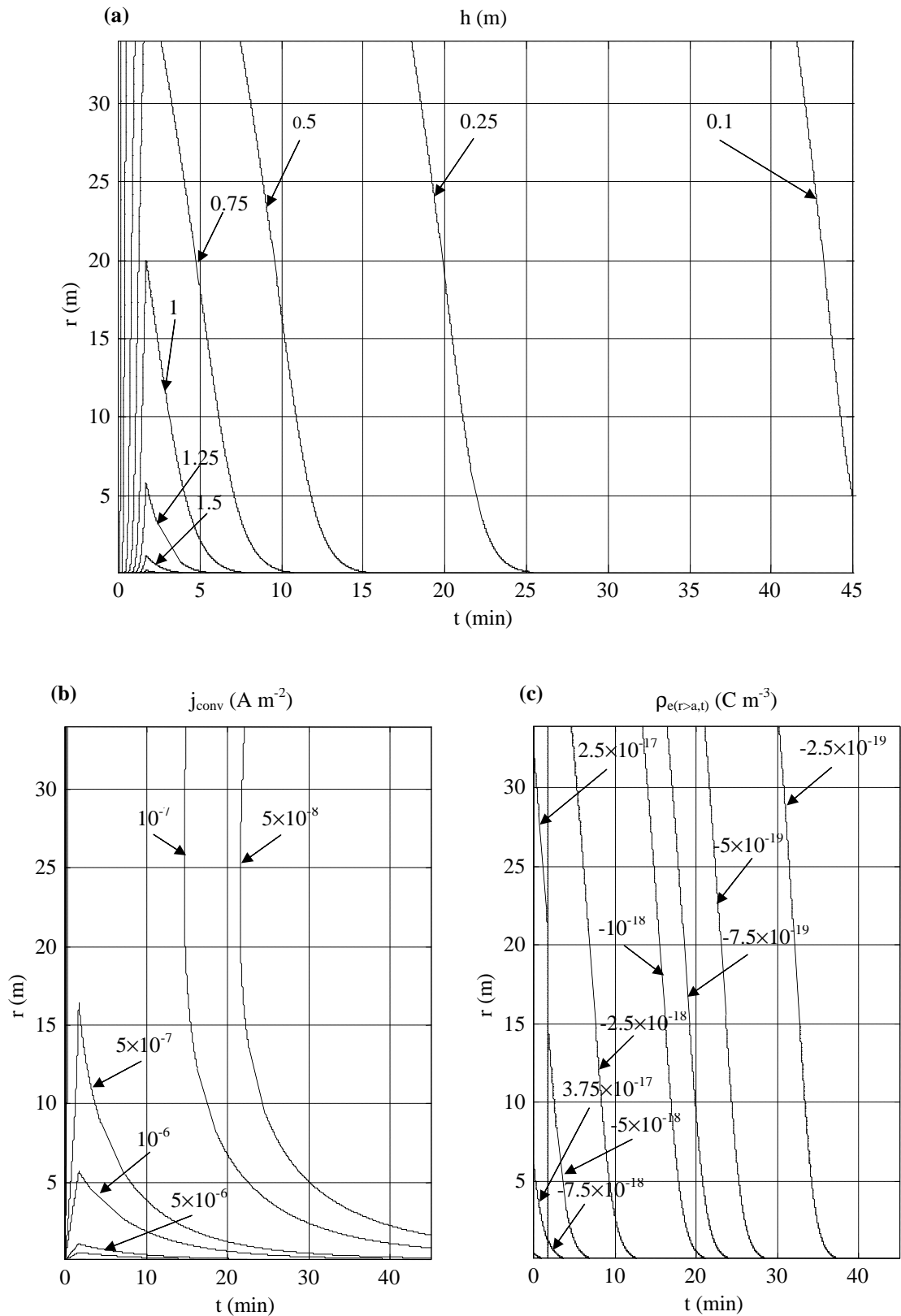


Figure 8

(a) Hydraulic head derived from Eq. (8) and $S_{seq} = 3.25 \times 10^{-6}\ m^{-1}$ and $K_{eq} = 10^{-5}\ m\ s^{-1}$. (b) Convection electrical current derived from Eq. (1), the definition of the hydraulic head and $h_{(r,t)}$ curves of Fig. 8a. (c) Equivalent electric charge density derived from Eq. (11) and $h_{(r,t)}$ curves of Fig. 8a.

when the water is pumped, and negative the rest of time (Fig. 8c). An opposite surface electric charge develops at the interface of the altered zone and the borehole so that the total electric charge is always equal to zero. The electric charge Q_0 corresponding to this surface electric charge is equal to the mean time of the volume integral of $\mathbf{r}_{e(r,t)}$ in the altered zone during the pumping cycles minus the pumping periods

$$Q_0 = \frac{1}{2705 - 102} \times \int_{t \in [102; 2705]} \left\{ \int_{r \in [0.0825; +\infty]} \int_{\mathbf{q} \in [0; 2\mathbf{p}]} \int_{z \in [0; 8]} \mathbf{r}_{e(r,t)} \times dr \times rd\mathbf{q} \times dz \right\} \times dt. \quad (12)$$

In the case where there are two boreholes, the situation is more complex. While the surface electric charge that develops at the interface of the altered zone and the boreholes is unchanged, the volume electric charge $\mathbf{r}_{e2boreholes(r,q,t)}$ that appears in the altered zone is the algebraic sum of the volume electric charge $\mathbf{r}_{e \text{ borehole } 1(r_1,t)}$ that is generated there by the first borehole, and the volume electric charge $\mathbf{r}_{e \text{ borehole } 2(r_2,t)}$ (of opposite sign) that is generated at the same place by the other borehole (Fig. 10). A priori, $\mathbf{r}_{e \text{ borehole } 1(r_1,t)}$ and $\mathbf{r}_{e \text{ borehole } 2(r_2,t)}$ cannot be derived from $\mathbf{r}_{e(r,t)}$ calculated with Eq. (11) and $h_{(r,t)}$ curves calculated with Eq. (8), since the presence of the two boreholes prevents the assumption of axial symmetry made in Eq. (8) from being valid. Yet, as noted before, the characteristic length of the excitation (*i.e.* the induced hydraulic head step, 10 m) is large compared to the influence distance between one borehole and the other (34 m), so $\mathbf{r}_{e(r,t)}$ can be used for calculating $\mathbf{r}_{e \text{ borehole } 1(r_1,t)}$ and $\mathbf{r}_{e \text{ borehole } 2(r_2,t)}$, provided that the integration is limited to the area between the boreholes ($X \in [\pm 17]$ m, see Fig. 10), where the fluid flow is mainly restricted in the steady-state regime. The resultant electric charge thus follows

$$Q_1 = \frac{1}{2705 - 102} \times \int_{t \in [102; 2705]} 2 \times \left\{ \int_{X \in [0; 17]} \int_{z \in [0; 8]} \left[\mathbf{r}_{e \text{ borehole } 1}(r_1,t) - \mathbf{r}_{e \text{ borehole } 2}(r_2,t) \right] \times dr \times rd\mathbf{q} \times dz \right\} \times dt \quad (13)$$

where r_1 , r_2 and X are given Fig. 10.

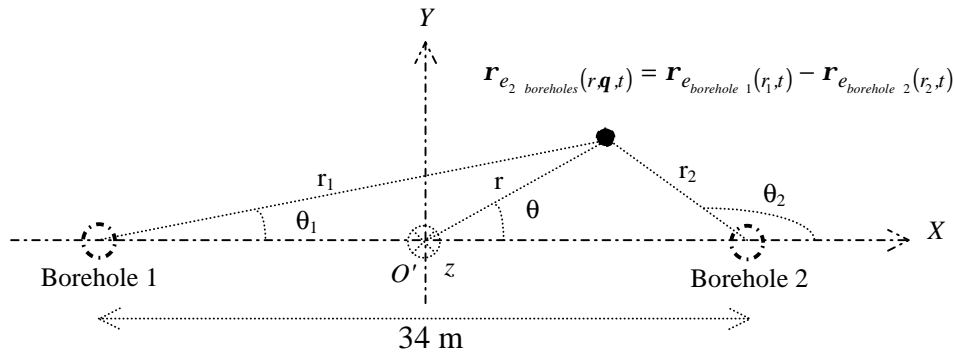


Figure 10

Geometrical conventions for the calculation of the electric charge that develops in the altered zone in case of two boreholes (viewed from above).

In practice, we truncated the integration in r (respectively \mathbf{q}) to $[0; 17]$ m (respectively $[0; \pi/2]$ Rad), so the given value of Q_1 is an underestimate of its real value by at most the ratio between the total surface that should have been taken into consideration in the integration and the surface that has actually been taken into consideration, that is 3.

Q_0 and Q_1 can be concentrated at the barycenter positions of $\mathbf{r}_{e(r,t)}$ and $\mathbf{r}_{e2\ boreholes(r,q,t)}$ for the estimation of their effect at the surface, far away from the sources. With $\mathbf{r}_{e(r,t)}$ of Fig. 8c and Eqs. (12) and (13), we found that Q_0 is equal to 8.2×10^{-15} C and concentrated at the center of the boreholes, while Q_1 is equal to 7.3×10^{-16} C and concentrated 4.4 m from the center of the boreholes. The corresponding electric quadrupole is given Fig. 11.

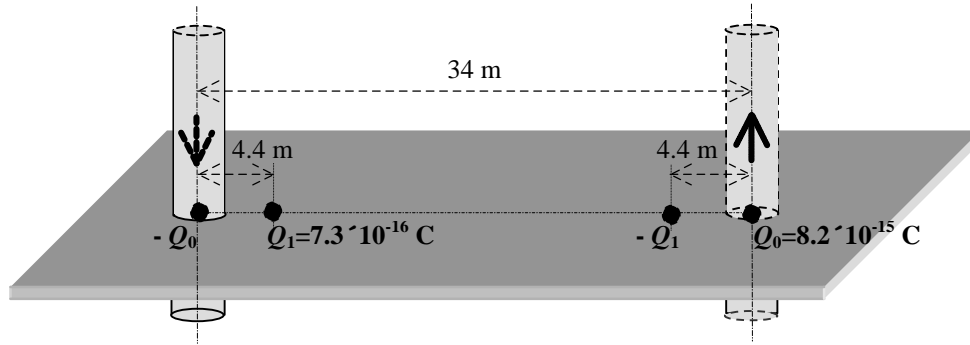


Figure 11

Schematic representation of the electric quadrupole that contributes to the electric potential measured with the surface electrodes.

The last step in the modeling consists of estimating how the electric potential generated at depth can reach the surface. In the nucleation zone of an impending earthquake, few data are generally available to constrain the electric structure. The medium is generally assumed to be either homogeneous or horizontally stratified. We thus decided to neglect, in the *a priori* model of Le Mayet de Montagne, the vertical electric conductivity contrast between the conductive boreholes and the resistive embedding rocks. The medium was rather assumed to be horizontally stratified, with an electric conductivity of 10^{-4} S m^{-1} down to 150 m (typical conductivity for a granite, see *e.g.* GUÉGUEN and PALCIAUSKAS, 1994), 3.2×10^{-2} S m^{-1} between 150 and 158 m (conductivity of the water measured in the field), and 10^{-4} S m^{-1} below. With these assumptions, we found (see Appendix for details of the calculation) that the voltage difference generated by the model is equal to 1 μ V for ERR0-ENE1 and ERR0-ESW1, and 10 μ V for ESW1-EB32 and ESW1-EB31 (Fig. 12). These values are much smaller than what was actually measured in the field, by a factor of about -5,000 for ERR0-ENE1, 8,000 for ERR0-ESW1 and 250 for ESW1-EB32 and ESW1-EB31.

4. Discussion

The assumption consisting of concentrating the electric charges at the density barycenters is not realistic for the estimation of the effect of the targeted streaming potential source 17 m above it, at 137 m depth. The discrepancy observed between the data recorded with ESW1-EB32 and ESW1-EB31 and the model predictions there are thus due to the fact that our simplifications are too crude at depth. The signals recorded with ESW1-EB32 and ESW1-EB31 therefore attest that a streaming potential source located at 155 m depth has actually been activated. The question is thus whether the source that created the surface observations is the deep targeted one, or another one, incidently activated.

Two phenomena were neglected in the *a priori* model and maybe led us to underestimate the electric field generated at the surface. First, we did not take the vertical resistivity contrasts that exist between the boreholes (which were full of water, and hence rather conductive) and the surrounding rocks (dry and resistive) into consideration in the model. Such contrasts are known to trap the electric field between the source and the surface, and to enhance the induced effects at the surface (see, *e.g.*, ISHIDO and PRITCHETT, 1999). WURMSTICH and MORGAN (1994) quantified this effect when they studied the impact of casings on steady-state streaming potentials generated by standard oil well pumping (about 500 m^3 day^{-1}) in typical North American reservoirs (100 m wide, 150 mD permeable, and 50 Ω resistive at 500 m depth). They showed that the distortions induced by the casings on the surface electric potential contour lines are restricted to the vicinity of the borehole heads, within regions delimited by at most 10 times the boreholes radii (WURMSTICH and MORGAN, 1994, Fig. 3). In the Mayet de Montagne, the radii of the boreholes was equal to about 10 cm, and the electrodes were located at least 17 m from the borehole heads. The effect of the vertical resistivity contrasts, if it existed, was thus limited to at most 1 m around the borehole heads, so that it is very unlikely to have generated the 5 or 8 mV monitored with ERR0-ENE1 and ERR0-ESW1.

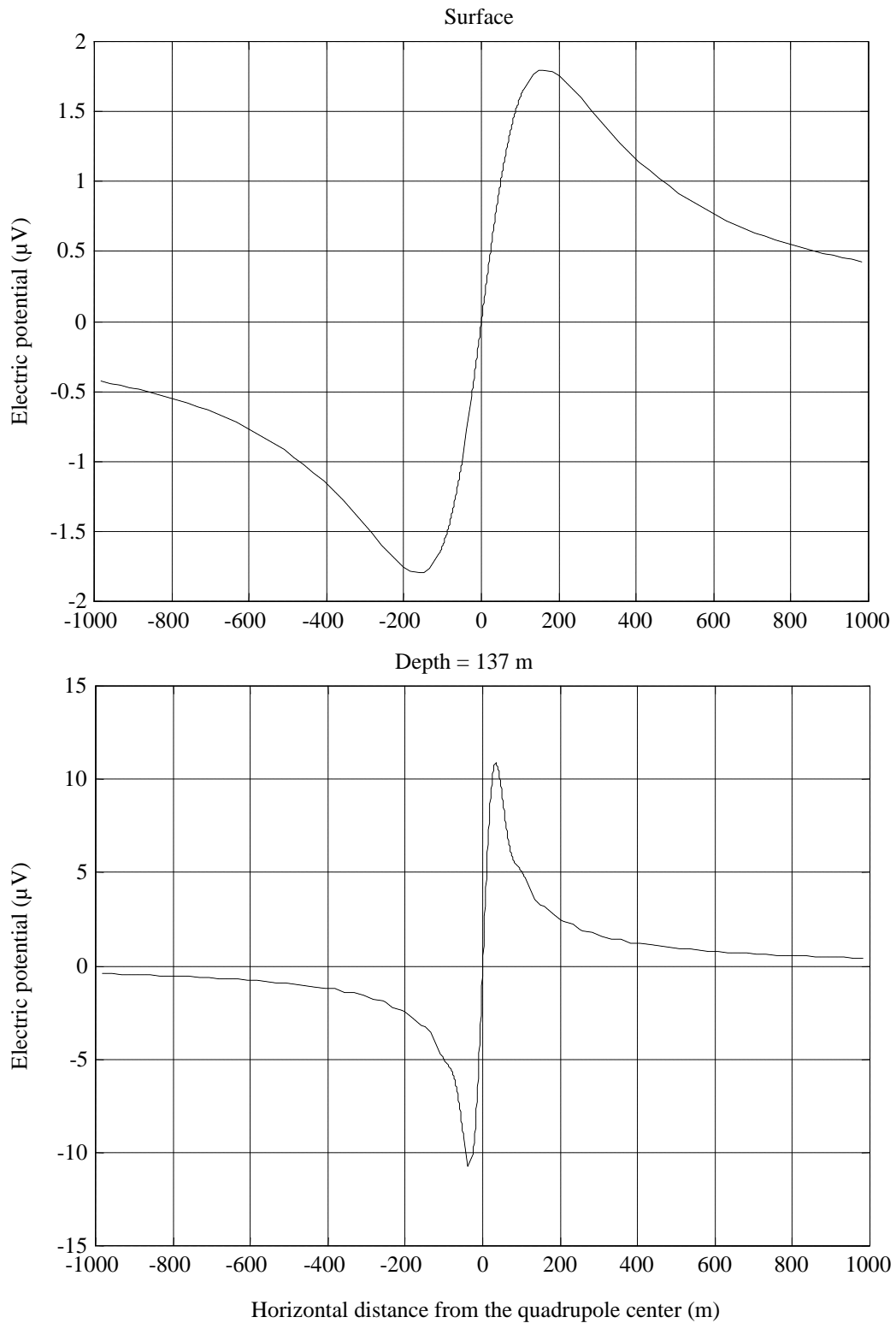


Figure 12

Electric potential expected at the surface and at depth by the electric quadrupole of Fig. 11 embedded in a horizontally stratified medium with an electric conductivity of 10^{-4} S m^{-1} down to 150 m, $3.2 \times 10^{-2} \text{ S m}^{-1}$ between 150 and 158 m (measured directly in the field), and 10^{-4} S m^{-1} below.

The second effect that may have led us underestimate the surface electric field is the fact that fluid flow leakages gathering up to 20% of the total fluid flow between boreholes III-2 and III-3 are known to occur close to the water table heads (CORNET, personal communication, 1996). These leakages may have created smaller but shallower streaming potential sources. Few constraints are available regarding the location and geometry of the fractures that interconnect boreholes III-2, III-3 and III-8. We know from visual coring analysis in borehole III-4 that altered granite is present from 6 to 8 m down in this borehole. Fig. 13 we test a plausible electro-kinetic

leakage source, that we associate with this fracture zone. We suppose that a 2-D horizontal fracture of 500 μm width is present 6 m below the surface, and generates an electric dipole of 1.75×10^{-15} C, representing 20% of the charge *a priori* induced at depth. In order not to have a zero signal at ERR0, we locate the negative charge below borehole III-8 and the positive charge about 5 m to the north-east of electrode ERR0. The electric potential generated at the surface has then a larger maximum amplitude than the previous one, but it is more concentrated in space (Fig. 13). The potential expected at ERR0 is equal to 4 mV and the voltage differences ERR0-ENE1 and ERR0-ESW1 are equal to 0.3 and 0.5 mV. These signs are in agreement with the measurements, while the amplitudes are 15 times lower than the measurements. With a small displacement of one of the charges towards electrode ERR0, or with the assumption that the fracture is 3-D and not 2-D, it is possible to generate the measured surface electric potential. It is possible, therefore, that the observations made at the surface were dominated by shallow fluid flow leakages.

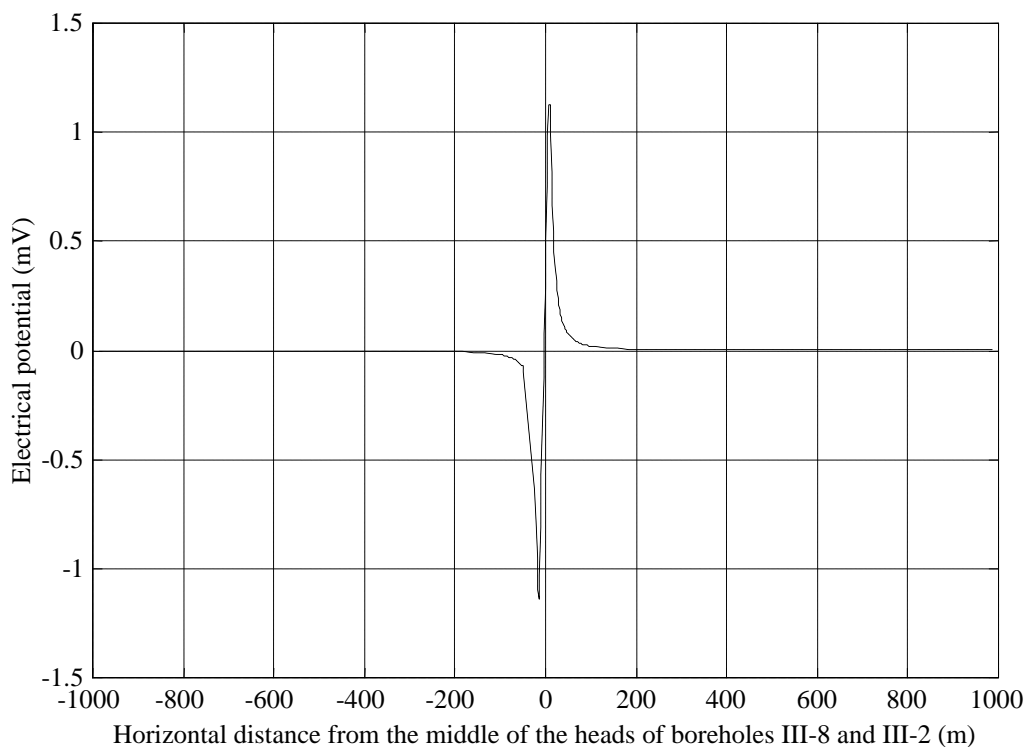


Figure 13

Electric potential expected at the surface by a horizontal electric dipole of charge $Q = 1.75 \times 10^{-15}$ C and length 22.5 m embedded at 6 m depth in a horizontally stratified medium with an electric conductivity of 10^{-4} S m^{-1} down to 6 m – 250 μm , 3.2×10^{-2} S m^{-1} between 6 m – 250 μm and 6 m + 250 μm , and 10^{-4} S m^{-1} below.

The effects of the shallow electric source at depth are very small. In particular, they are smaller close to electrodes EB31 and EB32 than that of the previous source. The electric potentials measured in borehole III-3 were thus dominated by the deeply activated streaming potential source.

5. Conclusion

The main aim of the study was to determine whether streaming potentials generated at depth can, in practice, be detected with a surface electrode network. We induced overpressures of 0.1 MPa at 150 m depth in a sub-horizontal granite fractured zone, and measured the electric potential at the surface and at depth. The permanent fluid flow regime was reached after one day, indicating a hydraulic conductivity of 10^{-5} m s^{-1} and a specific storage coefficient of 3.25×10^{-6} m^{-1} . An electric potential of about 5 mV was detected in association with the induced fluid flow. We modeled the streaming potentials associated with the hydraulic excitation, and found that a surface signal about 5,000 times smaller than the measurements was expected. The uncertainties associated with the model are too small to explain the discrepancy. The electric potentials detected at the surface were thus generated by another electric source, incidentally activated. We tested the effect of a very shallow source (6 m depth), associated with fluid flow leakages that are known to occur in the site, close to the water table heads. We found that it generates a surface electric potential compatible with the measurements. Therefore, it was considered likely that the observed surface electric potential was dominated by shallow fluid flow leakage.

Two electrodes were installed at depth, in the vicinity of the targeted deep streaming potential source. They recorded a signal associated with the forced fluid flow, and obviously due to the targeted deep streaming potential source.

It is consequently an established fact that, although we did activate a deep streaming potential source, our surface measurements were dominated by a smaller but shallower source, incidentally activated. This result thus illustrates the intrinsic difficulty of detecting streaming potentials generated at depth with surface electrode network, in particular in fractured areas where side sources like our leakage source are expected to be numerous. It also points out that detecting streaming potentials in a farm land is very difficult because of the high electric noise generated by the electric fences present in the vicinity.

BERNARD (1992) estimated the surface electric potential induced by plausible streaming potentials associated with hypothesized pre-seismic strains. He showed that the electric potential decays very rapidly with distance (as the inverse of the square of the distance), and cannot propagate far horizontally unless adequate horizontal channels are present between the source and the electrodes. We now add that electric potential is likely to be distorted by smaller but shallower streaming potentials triggered by fluid flows on adjacent faults or fractures. Such side-sources are expected to be numerous in the vicinity of major active fault zones, since the distribution of fault sizes in such regions is known to be fractal. Models of possible electrical earthquake precursors thus turn out to be more speculative than expected. In particular, even though it remains possible that assumed pre-seismic strains could sometimes generate detectable streaming potentials at the surface, using surface electrode networks to locate such sources appears to be very difficult.

Appendix: electric potential in a horizontally stratified medium

Following BERNARD (1992) and PINETTES *et al.* (1998), we found that the electric potential generated by a unipolar electrical current I buried at the depth z_0 in a stratified conductive medium consisting of two horizontal layers of conductivities \mathbf{s}_1 from $H = 0$ down to H_1 , and \mathbf{s}_2 from H_1 down to H_2 , lying over a half-space of conductivity \mathbf{s}_3 follows

$$V_{(r,z=0,z_0 \in [0,H_1])} = \frac{I}{2\pi\mathbf{s}_1} \times \int_0^{+\infty} J_0(kr) \times \frac{(1+R') \times sh[k(H_1 - z_0)] + \frac{\mathbf{s}_1}{\mathbf{s}_2} \times (1-R') \times ch[k(H_1 - z_0)]}{(1+R') \times ch(kH_1) + \frac{\mathbf{s}_1}{\mathbf{s}_2} \times (1-R') \times sh(kH_1)} \times dk \quad (14-a)$$

$$V_{(r,z \in [0,z_0], z_0 \in [0,H_1])} = \frac{I}{2\pi\mathbf{s}_1} \times \int_0^{+\infty} J_0(kr) \times \frac{(1+R') \times sh[k(H_1 - z_0)] + \frac{\mathbf{s}_1}{\mathbf{s}_2} \times (1-R') \times ch[k(H_1 - z_0)]}{(1+R') \times ch(kH_1) + \frac{\mathbf{s}_1}{\mathbf{s}_2} \times (1-R') \times sh(kH_1)} \times ch(kz) \times dk \quad (14-b)$$

$$V_{(r,z \in [z_0,H_1], z_0 \in [0,H_1])} = \frac{I}{4\pi\mathbf{s}_1} \times \frac{1}{\sqrt{r^2 + (z - z_0)^2}} + \frac{I}{2\pi\mathbf{s}_1} \times \int_0^{+\infty} J_0(kr) \times \left\{ \frac{(1+R') \times sh[k(H_1 - z_0)] + \frac{\mathbf{s}_1}{\mathbf{s}_2} \times (1-R') \times ch[k(H_1 - z_0)]}{(1+R') \times ch(kH_1) + \frac{\mathbf{s}_1}{\mathbf{s}_2} \times (1-R') \times sh(kH_1)} \times ch(kz) - \frac{e^{-kz_0}}{2} \times e^{kz} \right\} \times dk \quad (14-c)$$

$$\begin{aligned}
V_{(r,z \in [H_1, H_2], z_0 \in [0, H_1])} &= \frac{I}{2\mathbf{ps}_2} \times \int_0^{+\infty} J_0(kr) \\
&\times \left\{ \frac{\left[ch[k(H_1 - z_0)] \times ch(kH_1) - \frac{1-R'}{1+R'} \times sh[k(H_1 - z_0)] \times sh(kH_1) \right] \times e^{kH_1}}{(1+R') \times ch(kH_1) + \frac{\mathbf{S}_1}{\mathbf{S}_2} \times (1-R') \times sh(kH_1)} \times e^{-kz} \right. \\
&\left. - \frac{\left[ch[k(H_1 - z_0)] \times ch(kH_1) - \frac{1-R'}{1+R'} \times sh[k(H_1 - z_0)] \times sh(kH_1) \right] \times R' \times e^{-kH_1}}{(1+R') \times ch(kH_1) + \frac{\mathbf{S}_1}{\mathbf{S}_2} \times (1-R') \times sh(kH_1)} \times e^{kz} \right\} \times dk \quad (14-d)
\end{aligned}$$

$$\begin{aligned}
V_{(r,z \in [H_2, +\infty], z_0 \in [0, H_1])} &= \frac{I}{2\mathbf{ps}_3} \times \int_0^{+\infty} J_0(kr) \times \\
&\left\{ \frac{(1+R) \times ch[k(H_1 - z_0)] \times ch(kH_1) - \frac{(1-R') \times (1+R)}{1+R'} \times sh[k(H_1 - z_0)] \times sh(kH_1)}{(1+R') \times ch(kH_1) + \frac{\mathbf{S}_1}{\mathbf{S}_2} \times (1-R') \times sh(kH_1)} \right\} \times e^{kH_1} \\
&\times e^{-kz} \times dk, \quad (14-e)
\end{aligned}$$

when $0 \leq z_0 \leq H_1$,

$$V_{(r,z=0, z_0 \in [H_1, H_2])} = \frac{I}{2\mathbf{ps}_2} \times \int_0^{+\infty} J_0(kr) \times \frac{\left[e^{-k(z_0-H_1)} - R' e^{k(z_0-H_1)} \right]}{(1+R') \times ch(kH_1) + \frac{\mathbf{S}_1}{\mathbf{S}_2} \times (1-R') \times sh(kH_1)} \times dk \quad (15-a)$$

$$V_{(r,z \in [0, H_1], z_0 \in [H_1, H_2])} = \frac{I}{2\mathbf{ps}_2} \times \int_0^{+\infty} J_0(kr) \times \frac{\left[e^{-k(z_0-H_1)} - R' e^{k(z_0-H_1)} \right]}{(1+R') \times ch(kH_1) + \frac{\mathbf{S}_1}{\mathbf{S}_2} \times (1-R') \times sh(kH_1)} \times ch(kz) \times dk \quad (15-b)$$

$$\begin{aligned}
V_{(r,z \in [H_1, H_2], z_0 \in [H_1, H_2])} &= \frac{I}{4\mathbf{ps}_2} \times \frac{1}{\sqrt{r^2 + (z - z_0)^2}} \\
&+ \frac{I}{4\mathbf{ps}_2} \times \int_0^{+\infty} J_0(kr) \times \left\{ \frac{\left[e^{-k(z_0-2H_1)} - R' e^{kz_0} \right] \times \left[ch(kH_1) - \frac{\mathbf{S}_1}{\mathbf{S}_2} \times sh(kH_1) \right]}{(1+R') \times ch(kH_1) + \frac{\mathbf{S}_1}{\mathbf{S}_2} \times (1-R') \times sh(kH_1)} \times e^{-kz} \right. \\
&\left. - \frac{2R' e^{-2kH_1} \times \left[ch[k(z_0 - H_1)] \times ch(kH_1) + \frac{\mathbf{S}_1}{\mathbf{S}_2} \times sh[k(z_0 - d_1)] \times sh(kH_1) \right]}{(1+R') \times ch(kH_1) + \frac{\mathbf{S}_1}{\mathbf{S}_2} \times (1-R') \times sh(kH_1)} \times e^{kz} \right\} \times dk \quad (15-c)
\end{aligned}$$

$$\begin{aligned}
V_{(r,z \in [H_2, +\infty], z_0 \in [H_1, H_2])} &= \frac{I}{2\mathbf{ps}_2} \times \int_0^{+\infty} J_0(kr) \times e^{-kH_2} \times (e^{kH_1} - R) \\
&\times \frac{\left\{ ch[k(z_0 - H_1)] \times ch(kH_1) + \frac{\mathbf{S}_1}{\mathbf{S}_2} \times sh[k(z_0 - H_1)] \times sh(kH_1) \right\}}{(1+R') \times ch(kH_1) + \frac{\mathbf{S}_1}{\mathbf{S}_2} \times (1-R') \times sh(kH_1)} \times e^{-kz} dk, \quad (15-d)
\end{aligned}$$

when $H_1 \leq z_0 \leq H_2$,

$$V_{(r,z=0,z_0 \in [H_2, +\infty])} = \frac{I}{\mathbf{p}(\mathbf{s}_2 + \mathbf{s}_3)} \times \int_0^{+\infty} J_0(kr) \times \frac{e^{-k(z_0 - H_1)}}{(1 + R') \times ch(kH_1) + \frac{\mathbf{s}_1}{\mathbf{s}_2} \times (1 - R') \times sh(kH_1)} \times dk \quad (16-a)$$

$$V_{(r,z \in [0, H_1], z_0 \in [H_2, +\infty])} = \frac{I}{\mathbf{p}(\mathbf{s}_2 + \mathbf{s}_3)} \times \int_0^{+\infty} J_0(kr) \times \frac{e^{-k(z_0 - H_1)}}{(1 + R') \times ch(kH_1) + \frac{\mathbf{s}_1}{\mathbf{s}_2} \times (1 - R') \times sh(kH_1)} \times ch(kz) \times dk \quad (16-b)$$

$$V_{(r,z \in [H_1, H_2], z_0 \in [H_2, +\infty])} = \frac{I}{2\mathbf{p}(\mathbf{s}_2 + \mathbf{s}_3)} \times \int_0^{+\infty} J_0(kr) \times \left\{ \frac{\left[ch(kH_1) + \frac{\mathbf{s}_1}{\mathbf{s}_2} \times \frac{3 - R'}{1 + R'} \times sh(kH_1) \right] \times e^{-k(z_0 - 2H_1)}}{(1 + R') \times ch(kH_1) + \frac{\mathbf{s}_1}{\mathbf{s}_2} \times (1 - R') \times sh(kH_1)} \times e^{-kz} \right. \\ \left. + \frac{\left[ch(kH_1) + \frac{\mathbf{s}_1}{\mathbf{s}_2} \times \frac{1 - 3R'}{1 + R'} \times sh(kH_1) \right] \times e^{-kz_0}}{(1 + R') \times ch(kH_1) + \frac{\mathbf{s}_1}{\mathbf{s}_2} \times (1 - R') \times sh(kH_1)} \times e^{kz} \right\} \times dk \quad (16-c)$$

$$V_{(r,z \in [H_2, +\infty], z_0 \in [H_2, +\infty])} = \frac{I}{4\mathbf{p}\mathbf{s}_3} \times \frac{1}{\sqrt{r^2 + (z - z_0)^2}} \\ + \frac{I}{2\mathbf{p}(\mathbf{s}_2 + \mathbf{s}_3)} \times \int_0^{+\infty} J_0(kr) \times \left\{ \left[e^{2kH_1} + e^{-2kH_2} - \frac{\mathbf{s}_2 + \mathbf{s}_3}{2\mathbf{s}_3} \times (1 + R') \times e^{2kH_2} \right] \times ch(kH_1) \right. \\ \left. + \frac{\mathbf{s}_1}{\mathbf{s}_2} \times \left[(3 - R') \times e^{2kH_1} + \frac{1 - 3R'}{1 + R'} \times e^{-2kH_2} - \frac{\mathbf{s}_2 + \mathbf{s}_3}{2\mathbf{s}_3} \times (1 - R') \times e^{2kH_2} \right] \times sh(kH_1) \right\} \\ \left. / \left\{ (1 + R') \times ch(kH_1) + \frac{\mathbf{s}_1}{\mathbf{s}_2} \times (1 - R') \times sh(kH_1) \right\} \times e^{-kz_0} \times e^{-kz} \times dk \quad (16-d)$$

when $H_2 \leq z_0$, with

$$R = \frac{\mathbf{s}_3 - \mathbf{s}_2}{\mathbf{s}_2 + \mathbf{s}_3}, \quad (17-a)$$

$$R' = R \times e^{-2k(H_2 - H_1)} \quad (17-b)$$

where J_n and Y_n are the Bessel function of the first kind and second kind, respectively, of the order n .

The source codes for programs corresponding to these solutions of the Laplace equation as well as for Eq. (8) can be downloaded at the Royal Observatory of Belgium web site: <http://homepage.oma.be/patrickp/Softwares/Sources.html>.

Acknowledgments

We would like to thank Pierre Adler and Jean-Louis Le Mouël for their very fruitful advice when we tried to calculate the Bessel solutions of the Laplace function in the case where the studied property contrasts are vertical. We are also grateful to Dr. G. Olhoef and an anonymous referee for their constructive and helpful reviews. This work was supported by the DBT Thème “Fluides et Failles” and PNRN programs, INSU/CNRS,

as well as by the E.C. Environment and Climate Program, Topic Seismic Risk, Contracts #ENV4V-CT96-0276 and ENV4-CT97-5086. This is IPGP contribution 1755.

REFERENCES

- ADAMSON, A. W. (5th ed.), *Physical Chemistry of Surfaces* (Wiley-Interscience, New York, 1990).
- ADLER, P., J.-L. LE MOUËL, and J. ZLOTNICKI (1999), *Electrokinetic and magnetic fields generated by flow through a fractured zone: A sensitivity study for La Fournaise volcano*, *Geophys. Res. Lett.*, **26**, 795-798.
- BERNABÉ, Y. (1998), *Streaming potential in heterogeneous networks*, *J. Geophys. Res.*, **103**, 20,827-20,841.
- BERNARD, P. (1992), *Plausibility of models of electro-telluric anomalies observed at large distances from areas of earthquake preparation*, *J. Geophys. Res.*, **97**, 17,531-17,546.
- BERNARDI A., A. C. FRASER-SMITH, P. R. MCGILL, and O. G. VILLARD Jr. (1991), *ULF magnetic field measurements near the epicenter of the M_s 7.1 Loma Prieta earthquake*, *Phys. Earth Planet. Inter.*, **68**, 45-63.
- CARLSAW, H. S. and J. C. JAEGER (2nd ed.), *Conduction of heat in solid* (Charendon Press, Oxford, 342-344, 1986).
- CORNET, F., H., *Expérimentation à faible profondeur sur une méthode d'exploitation de la chaleur des roches profondes peu perméables, Volume 1*, (Rapport final pour le contrat CEE EGD-1-002 F, CEE, Bruxelles, 1984).
- CORNET, F., H., *Projet Mayet de Montagne: Étude in situ de la percolation forcée d'eau en milieu granitique* (Rapport final Géothermie Profonde Généralisée, CNRS, Paris, 1988).
- DE GROOT, S. R. and P. MAZUR, *Non equilibrium thermodynamics* (Elsevier, Amsterdam, 405-452, 1962).
- DE MARSILY, G., *Quantitative hydrogeology – Groundwater hydrology for engineers* (Academic Press, San Diego, 1986).
- FENOGLIO, M. A., A. C. FRASER-SMITH, G. C. BEROZA, and M. J. S. JOHNSTON (1993), *Comparison of ultra-low frequency electromagnetic signals with aftershock activity during the 1989 Loma Prieta earthquake sequence*, *Bull. Seism. Soc. Am.*, **83**, 347-357.
- FENOGLIO, M. A., M. J. S. JOHNSTON (1995), *Magnetic and electric fields associated with changes in high pore pressure in fault zones – Application to the Loma Prieta ULF emissions*, *J. Geophys. Res.*, **100**, 12,951-12,958.
- FRASER-SMITH, A. C., A. BERNARDI, P. R. MCGILL, M. E. LADD, R. A. HELLIWELL, and O. G. VILLARD Jr. (1990), *Low-frequency magnetic field measurements near the epicenter of the M_s 7.1 Loma Prieta earthquake*, *Geophys. Res. Lett.*, **17**, 1465-1468.
- GELLER, R. J. Ed (1996), *Debate on "VAN"*, *Geophys. Res. Lett.*, **23**, 1291-1452.
- GRUSZOW, S., J.-C. ROSSIGNOL, A. TZANIS, and J.-L. LE MOUËL (1996), *Identification and analysis of electromagnetic signals in Greece: The case of the Kozani earthquake VAN prediction*, *Geophys. Res. Lett.*, **23**, 2025-2028.
- GUÉGUEN, Y. and V. PALCIAUSKAS, *Introduction to the Physics of Rocks* (Princeton Univ. Press, Princeton, 1994).
- HASHIMOTO, T. and Y. TANAKA (1995), *A large self-potential anomaly on Unzen volcano, Shimabara peninsula, Kyushu island, Japan*, *Geophys. Res. Lett.*, **22**, 191-194.
- ISHIDO, T. and H. MIZUTANI (1981), *Experimental and theoretical basis of electrokinetic phenomena in rock-water systems and its application to geophysics*, *J. Geophys. Res.*, **86**, 1763-1775.
- ISHIDO, T., H. MIZUTANI, and K. BABA (1983), *Streaming potential observations, using geothermal wells and in situ electrokinetic coupling coefficient under high temperature*, *Tectonophysics*, **91**, 89-104.
- ISHIDO, T. and J. W. PRITCHETT (1999), *Numerical simulation of electrokinetic potentials associated with subsurface fluid flow*, *J. Geophys. Res.*, **104**, 12,247-12,259.
- JOHNSTON, M. J. S. (1997), *Review of electric and magnetic fields accompanying seismic and volcanic activity*, *Surveys Geophys.*, **18**, 441-475.
- JOUNIAUX, L. and J.-P. POZZI (1995), *Streaming potential and permeability of saturated sandstones under triaxial stress: Consequences for electro-telluric anomalies prior to earthquakes*, *J. Geophys. Res.*, **100**, 10,197-10,209.
- JOUNIAUX, L. and J.-P. POZZI (1997), *Laboratory measurements anomalous 0.1-0.5 Hz streaming potential under geochemical changes: Implications for electro-telluric precursors to earthquakes*, *J. Geophys. Res.*, **102**, 15,335-15,343.
- LIGHTHILL, SIR J. (Ed.), *A critical review of VAN – Earthquake prediction from Seismic Electric Signals*, (World Sci., River Edge, N. I., 1996).
- LORNE B., F. PERRIER, and J.-P. AVOUAC (1999a), *Streaming potential measurements: 1. Properties of the electrical double layer from crushed rock samples*, *J. Geophys. Res.*, **104**, 17,857-17,877.
- LORNE B., F. PERRIER, and J.-P. AVOUAC (1999b), *Streaming potential measurements: 2. Relationship between electrical and hydraulic flow patterns from rock samples during deformation*, *J. Geophys. Res.*, **104**, 17,879-17,886.
- MICHEL, S. and J. ZLOTNICKI (1998), *Self-potential and magnetic surveying of La Fournaise volcano (Réunion island): Correlations with faulting, fluid circulation, and eruption*, *J. Geophys. Res.*, **103**, 17,845-17,857.
- MORGAN, F. D., E. R. WILLIAMS, and T. R. MADDEN (1989), *Streaming Potential properties of Westerly Granite with applications*, *J. Geophys. Res.*, **94**, 12,449-12,461.
- PAPADOPOULOS, I. S. and H. H. COOPER Jr. (1967), *Drawdown in a well of large diameter*, *Water Resour. Res.*, **3**, 241-244.
- PARK, S. K., M. J. S. JOHNSTON, T. R. MADDEN, F. D. MORGAN, and H. F. MORRISON (1993), *Electromagnetic precursors to earthquakes in the U.L.F. band: A review of observations and mechanisms*, *Rev. Geophys.*, **31**, 117-132.
- PERRIER, F. E., G. PETIAU, G. CLERC, V. BOGORODSKY, E. ERKUL, L. JOUNIAUX, D. LESMES, J. MACNAE, J. M. MEUNIER, D. MORGAN, D. NASCIMENTO, G. OETTINGER, G. SCHWARZ, H. TOH, M. J. VALIANT, K. VOZOFF, and O. YAZICI-ÇAKIN (1997), *A one year study of electrodes for long period measurements of the electric field in geophysical environments*, *J. Geomag. Geoelectr.*, **49**, 1677-1696.
- PERRIER, F., M. TRIQUE, B. LORNE, J.-P. AVOUAC, S. HAUTOT, and P. TARITS (1998), *Electric potential variations associated with yearly lake level variations*, *Geophys. Res. Lett.*, **25**, 1955-1958.
- PHAM, v.-N., D. BOYER, G. CHOULIARAS, J.-L. LE MOUËL, J.-C. ROSSIGNOL, and G. N. STAVRAKAKIS (1998), *Characteristics of electromagnetic noise in the Ioannina region (Greece); a possible origin for so called "Seismic Electric Signal" (SES)*, *Geophys. Res. Lett.*, **25**, 2229-2232.

- PHAM, V.-N., D. BOYER, J.-L. LE MOUËL, G. CHOULIARAS, and G. N. STAVRAKAKIS (1999), *Electromagnetic signals generated in the solid Earth by digital transmission of radio-waves as a plausible source for some so-called "Seismic Electric Signal"*, *Phys. Earth Planet. Inter.*, 114, 141-163.
- PINETTES, P., P. BERNARD, J. ARTRU, P.-A. BLUM, R. VERHILLE, P. MILAS, and G. VEIS (1998), *Strain constraint on the source of the alleged VAN precursor of the 1995 Aigion earthquake*, *J. Geophys. Res.*, 103, 15,145-15,155.
- REVIL, A., P. A. PEZARD, and P. W. J. GLOVER (1999a), *Streaming potential in porous media 1. Theory of the zeta potential*, *J. Geophys. Res.*, 104, 20,021-20,031.
- REVIL, A., H. SCHWAEGER, L. M. CATHLES III, P. D. MANHARDT (1999b), *Streaming potential in porous media 2. Theory and application to geothermal systems*, *J. Geophys. Res.*, 104, 20,033-20,048.
- TRIQUE, M., P. RICHON, F. PERRIER, J.-P. AVOUAC, and J.-C. SABROUX (1999), *Radon emanation and electric potential variations associated with transient deformation in the vicinity of reservoir lakes*, *Nature*, 399, 137-141.
- WURMSTICH, B. and F. D. MORGAN (1994), *Modeling of streaming potential response by oil well pumping*, *Geophys.*, 59, 46-56.
- ZLOTNICKI, J. and J.-L. LE MOUËL (1990), *Possible electrokinetic origin of a large magnetic variations at La Fournaise volcano*, *Nature*, 343, 633-636.

(Received March 27, 2000, revised January 8, 2001, accepted April 14, 2001)